Mcl-1 involvement in mitochondrial dynamics is associated with apoptotic cell death

Giampaolo Morciano[a], Carlotta Giorgi[a], Dario Balestra[b], Saverio Marchi[a], Daniela Perrone[c], Mirko Pinotti[b], and Paolo Pinton[a]

[a]Department of Morphology, Surgery and Experimental Medicine, Section of Pathology, Oncology and Experimental Biology, Laboratory for Technologies of Advanced Therapies, [b]Department of Life Sciences and Biotechnology, and [c]Department of Chemical and Pharmaceutical Sciences, University of Ferrara, FE 44121 Ferrara, Italy

ABSTRACT **The B-cell lymphoma-2 (Bcl-2) family proteins are critical regulators of apoptosis and consist of both proapoptotic and antiapoptotic factors. Within this family, the myeloid cell leukemia factor 1 (Mcl-1) protein exists in two forms as the result of alternative splicing. The long variant (Mcl-1L) acts as an antiapoptotic factor, whereas the short isoform (Mcl-1S) displays proapoptotic activity. In this study, using splice-switching antisense oligonucleotides (ASOs), we increased the synthesis of Mcl-1S, which induced a concurrent reduction of Mcl-1L, resulting in increased sensitivity of cancer cells to apoptotic stimuli. The Mcl-1 ASOs also induced mitochondrial hyperpolarization and a consequent increase in mitochondrial calcium (Ca^{2+}) accumulation. The high Mcl-1S/L ratio correlated with significant hyperfusion of the entire mitochondrial network, which occurred in a dynamin-related protein (Drp1)–dependent manner. Our data indicate that the balance between the long and short variants of the Mcl-1 gene represents a key aspect of the regulation of mitochondrial physiology. We propose that the Mcl-1L/S balance is a novel regulatory factor controlling the mitochondrial fusion and fission machinery.**

Monitoring Editor
Donald D. Newmeyer
La Jolla Institute for Allergy and Immunology

Received: Jan 16, 2015
Revised: Oct 28, 2015
Accepted: Oct 29, 2015

INTRODUCTION

More than 20 years ago, the identification and cloning of *Bcl-2* marked the discovery of an entirely new class of genes with crucial roles in cancer (Hanada *et al.*, 1993). The Bcl-2 family of proteins includes a great variety of members with proapoptotic (Bax, Bak, Bok, Bid, Bim, Noxa, Puma, myeloid cell leukemia factor 1 [Mcl-1] variant S) or antiapoptotic (B-cell lymphoma-2 [Bcl-2], Bcl-xL, Bcl-w, Mcl-1L) functions. They form homodimers and heterodimers through Bcl-2 homology (BH) domains. The relationships and relative ratios among the Bcl-2 family proteins are critical in cell fate determination (Boise *et al.*, 1995).

Mcl-1 was discovered based on its increased expression during cell commitment toward differentiation in a human myeloid leukemia cell line (Kozopas *et al.*, 1993). In humans, the Mcl-1 pre-mRNA undergoes alternative splicing (AS) to produce two isoforms with opposite functions. The first isoform, Mcl-1L, is primarily anchored by its transmembrane (TM) domain (Yang *et al.*, 1995) to the outer mitochondrial membrane (OMM), where it inhibits the release of cytochrome *c* (Clohessy *et al.*, 2006). Mcl-1L consists of 350 amino acids (aa) encoded by three exons. Bcl-2 and Mcl-1 share high similarity, especially in their carboxyl termini (C-ter), which terminate in a hydrophobic domain with membrane-spanning potential (Kozopas *et al.*, 1993). The similarities between these two genes are highly significant, although Mcl-1L and Bcl-2 are clearly distinguishable, except for two nearly identical stretches (7 aa each). The amino terminus (N-ter) of Mcl-1L differs from that of Bcl-2 in that it contains regions of low sequence complexity and sequences rich in proline, glutamic acid, serine, and threonine residues, which are often found in proteins that are rapidly turned over by the proteasome (Hershko and Ciechanover, 1998). As a result, unlike other Bcl-2 family members, the Mcl-1L protein is extremely unstable and has a very short

This article was published online ahead of print in MBoC in Press (http://www.molbiolcell.org/cgi/doi/10.1091/mbc.E15-01-0028) on November 4, 2015.

Address correspondence to: Paolo Pinton (paolo.pinton@unife.it).

Abbreviations used: AEQ, aequorin; AS, alternative splicing; ASO, antisense oligonucleotide; BH, Bcl-2 homology domain; cyt, cytosolic; Drp1, dynamin-related protein 1; ER, endoplasmic reticulum; ESE, exonic splicing enhancer; FCCP, carbonyl cyanide 4-(trifluoromethoxy) phenylhydrazone; IMM, inner mitochondrial membrane; IP_3, inositol 1,4,5 triphosphate; IP_3R, IP_3 receptor; Mcl-1, myeloid cell leukemia factor 1; MCU, mitochondrial Ca^{2+} uniporter; MOMP, mitochondrial outer membrane permeabilization; mt, mitochondrial; OMM, outer mitochondrial membrane; TM, transmembrane domain; TMRM, tetramethylrhodamine, methyl ester; Ψ_m, mitochondrial membrane potential.

half-life (1–3 h; Maurer *et al.*, 2006). The rapid induction and destruction of Mcl-1L has been proposed as a molecular mechanism for cells to switch between survival and apoptotic pathways in response to various stresses (Opferman *et al.*, 2003). Sequence analysis shows that Mcl-1L contains three putative BH domains: BH1–3. The BH2 domain allows Mcl-1 to heterodimerize with other Bcl-2 family members and is critical for antiapoptotic pathways (Yin *et al.*, 1994). In contrast, the BH3 motif has a prominent proapoptotic role (Kelekar and Thompson, 1998), especially in the presence of a direct activator of Bax or Bak (Kuwana *et al.*, 2005).

The second major splicing product of Mcl-1 arises from exon 2 skipping and encodes a 271-aa protein isoform called Mcl-1S. Compared with the longer variant, Mcl-1L, Mcl-1S lacks the BH1, BH2, and TM domains (Bae *et al.*, 2000; Bingle *et al.*, 2000) and is primarily localized to the cytosol. Although it occurs with low efficiency, Mcl-1 may undergo an additional AS event to produce an extrashort Mcl-1 form (Mcl-1ES) that interacts with Mcl-1L and induces the mitochondrial cell death pathway (Kim *et al.*, 2009).

Given the clear association between defective apoptosis and cancer and because Mcl-1 is often overexpressed in several types of human tumors (Derenne *et al.*, 2002; Khoury *et al.*, 2003; Placzek *et al.*, 2010; Perciavalle and Opferman, 2013), many attempts have been made to reestablish cellular sensitivity to apoptosis by modulating Mcl-1 expression.

Developments in the study of apoptosis have also uncovered a central role for mitochondrial morphology. Its influence has been observed for bioenergetic and redox homeostasis (Hackenbrock, 1966), Ca^{2+} regulation (Giorgi *et al.*, 2012), and cell life and death decisions (Scheckhuber, 2005), with mitochondrial shape influencing function and vice versa. A number of components of the fission and fusion machinery, including optic atrophy 1 (OPA1), Fis1, dynamin-related protein 1 (Drp1), mitofusin 1 (MFN1), and MFN2, have been directly implicated in the alteration of mitochondrial shape and thus in the regulation of apoptosis (James *et al.*, 2003; Frezza *et al.*, 2006), although often with apparently contradictory results. In this scenario, Drp1 has been suggested to be both a fundamental inducer of apoptosis (Frank *et al.*, 2001) and an inhibitor of Ca^{2+}-dependent apoptosis (Szabadkai *et al.*, 2004) by fragmenting the mitochondrial network into punctate units.

Although mitochondrial fusion has been associated with a healthy cell state because of matrix content exchanges (Chen *et al.*, 2005), it has recently been shown that fusion can also favor cell death (Westrate *et al.*, 2014). Additional evidence for this arises from the mitochondrial protein 18 kDa (MTP18), for which a reduction impairs mitochondrial morphology, increasing the interconnections among mitochondria and increasing the response to apoptotic stimuli (Tondera *et al.*, 2004).

Antisense oligonucleotides represent powerful tools for manipulating gene expression for therapeutic purposes and have been extensively exploited to knock down genes involved in cancer progression and therapeutic resistance (Gleave and Monia, 2005) and in a wide range of genetic disorders (Hadaschik *et al.*, 2008). In particular, the therapeutic potential of antisense oligonucleotide (ASO)–mediated Mcl-1L silencing has been shown in a variety of cancer cells, including blood cancer, melanoma (Skvara *et al.*, 2005), gastric cancer (Wacheck *et al.*, 2006), hepatocellular carcinoma (Sieghart *et al.*, 2006), and squamous cell carcinoma (Skoda *et al.*, 2008) cells, making Mcl-1L an important target in both liquid and solid tumors.

In addition, ASOs are emerging as promising tools to finely modulate gene expression by disrupting pre-mRNA splicing (splice-switching ASOs [sc-ASOs]). In this case, the strategy consists in using ASOs to mask splicing regulatory elements in the nascent pre-mRNA to alter exon inclusion or exclusion (Spitali and Aartsma-Rus, 2012). This strategy has been extensively explored to induce exon skipping as a therapy for human genetic disorders (Koo and Wood, 2013), and it also represents a valid option for cancer treatment (Bauman *et al.*, 2010).

Mcl-1 has features that suggest that it is an ideal target for therapeutic splicing modulation. For example, an sc-ASO-mediated shift of the isoform ratio toward proapoptotic Mcl-1S triggers cancer cell apoptosis and inhibits tumor development in mouse models (Shieh *et al.*, 2009; Kim *et al.*, 2011). However, the sc-ASOs tested thus far were designed to target Mcl-1L exon–intron junctions that are moderately conserved among human genes, thus potentially leading to off-target effects.

Driven by these considerations, we designed a novel Mcl-1–specific sc-ASO that could significantly reduce the Mcl-1L/S ratio and sensitize cells to apoptosis. For the first time, we demonstrated that the Mcl1S-mediated mechanism involves mitochondrial physiology, thus suggesting that the Mcl-1L/S balance is a critical regulator of mitochondrial morphology and dynamics.

RESULTS

Mcl-1 mRNA splicing pattern and protein expression

In view of the importance of Mcl-1 in determining apoptosis sensitivity, we measured the expression levels of both Mcl-1L and Mcl-1S in tumor cells.

HeLa cells have a significantly high level of Mcl-1L mRNA, as illustrated by the 689–base pair fragment from a reverse transcription (RT) PCR analysis (Figure 1A). As expected, the shorter isoform Mcl-1S (441 base pairs) is weakly expressed compared with the long variant. Western blot (WB) revealed that the protein counterparts of the two isoforms were expressed at comparable levels (Figure 1B). The discrepancy between mRNA and protein patterns may be due to the higher rate of proteasome-mediated turnover of the long form compared with that of the short form, which can be blocked by carbobenzoxy-Leu-Leu-leucinal (MG132) treatment (Figure 1C).

To promote a shift toward the proapoptotic form of Mcl-1 and investigate the underlying mechanism, we designed a panel of novel 2′-*O*-methyl phosphorothioate–based oligonucleotides targeting the putative exonic splicing enhancers (ESEs) of Mcl-1L exon 2 (Figure 1D). Treatment of HeLa cells with sc-ASO and subsequent RT-PCR analysis showed that only Mcl-1 sc-ASO3 (Mcl-1S3) induced an appreciable and dose-dependent effect with a shift toward the Mcl-1S form (Figure 1E). The capacity of Mcl-1S3 to decrease Mcl-1L protein production was then assessed by WB using protein lysates of HeLa cells 24 h after treatment (Figure 1F), which demonstrated a significantly lower level of Mcl-1L (40 kDa) compared with the untreated cells. The expression of the smaller protein (32 kDa) did not vary appreciably. This could be due to the labile nature and high instability of Mcl-1 (Chao *et al.*, 1998; Thomas *et al.*, 2010), which make its detection difficult.

Taken together, these results showed that steric interference of the ESE elements in the Mcl-1 exon 2 pre-mRNA by the newly designed Mcl-1S3 leads to exon skipping and a consequent increase in the expression of the short Mcl-1S protein isoform.

Shifting the dominant Mcl-1 variant from L to S reestablished sensitivity to apoptosis in HeLa cells

Next we evaluated whether modifying Mcl-1L pre-mRNA splicing with Mcl-1S3 could lead to an increase in apoptosis upon treatment with Ca^{2+}-dependent apoptotic stimuli. To test this hypothesis, we analyzed apoptosis by both WB analysis of two apoptotic markers, including cleaved poly(ADP)ribose polymerase (PARP) and

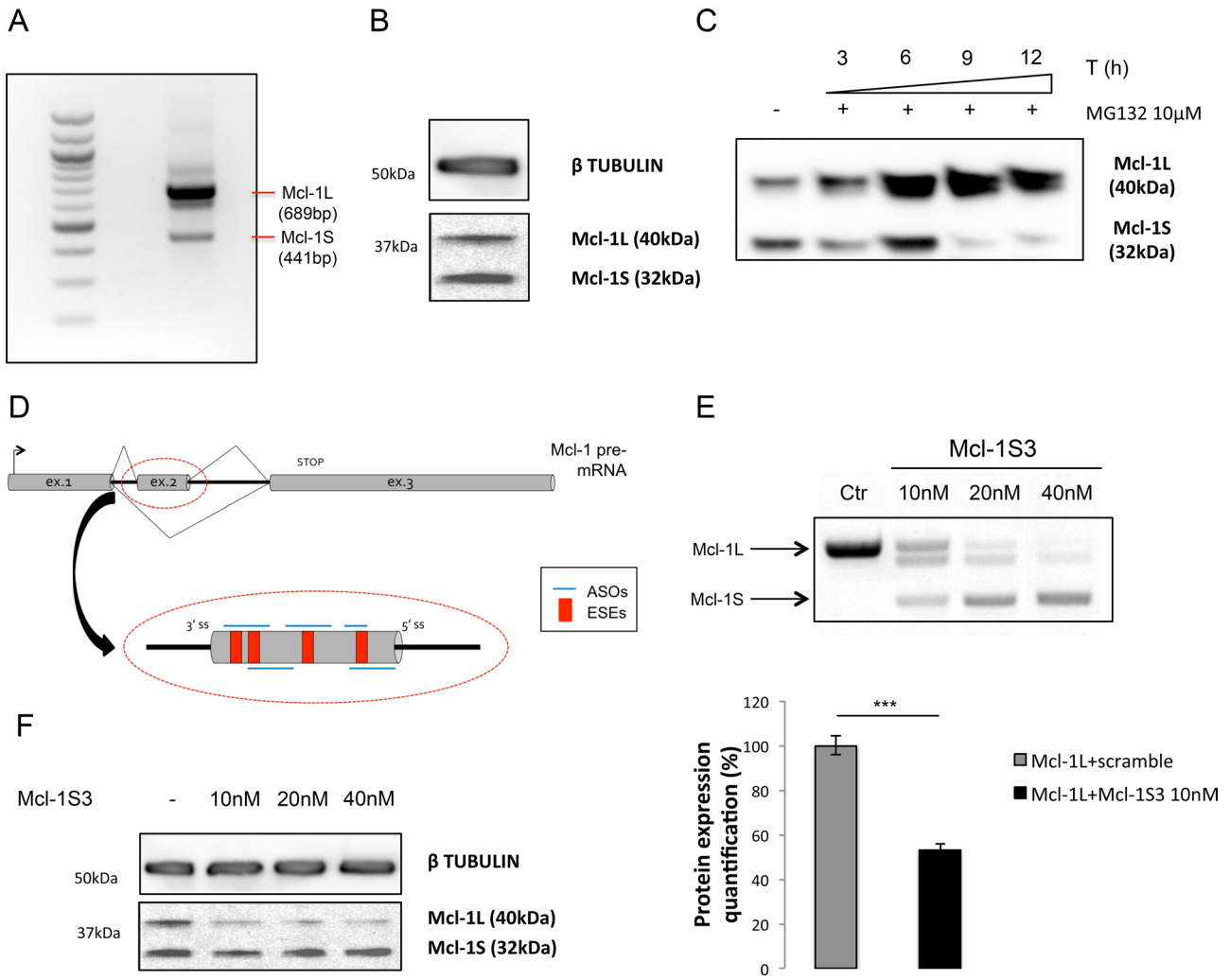

FIGURE 1: Mcl-1 mRNA splicing pattern and protein expression in control and experimentally treated HeLa cells. (A) Splicing pattern and (B) protein expression of Mcl-1 in control HeLa cells. (C) MG132 treatment from 3 to 12 h shows that Mcl-1L has a rapid turnover via proteasomal degradation. (D) Schematic illustration of the ASO double-stranded RNAs complementary to the ESEs of exon 2. (E) Splicing shifting from Mcl-1L to Mcl-1S after ASO transfection is dose dependent. (F) Relative protein expression levels. ***$p < 0.001$.

caspase 3, and annexin V staining. Treatment with Mcl-1S3 resulted in increased apoptotic cell death (Galluzzi *et al.*, 2015), as indicated by apoptosis markers (Figure 2A) and an increase in the number of annexin V–positive cells (Figure 2C). HeLa cells had increased susceptibility to menadione, ceramide, hydrogen peroxide, and thapsigargin when the Mcl-1S isoform was dominant. Of importance, Mcl-1S3 did not promote apoptosis with Ca^{2+}-independent stimuli, such as etoposide (Figure 2B).

These results indicated that the shift in splicing from Mcl-1L to Mcl-1S by Mcl-1S3 is a priming stimulus for extensive cell death through the mitochondrial intrinsic apoptotic pathway. The absence of appreciable cell death in untreated cells (Figures 2C and later discussion) upon Mcl-1S3 transfection is not likely due to a balancing mechanism activated by other antiapoptotic proteins, such as Bcl-2 and Bcl-XL, upon the loss of Mcl-1L protein (Figure 2D).

Mcl-1S3–induced imbalance in the Mcl-1L/S ratio altered mitochondrial Ca^{2+} homeostasis in HeLa cells

Given that Mcl-1L is primarily located on the outer mitochondrial membrane and Ca^{2+} is an important second messenger molecule involved in life and death decision pathways, we evaluated whether intracellular Ca^{2+} homeostasis was affected by the Mcl-1L/S imbalance.

For this purpose, we monitored Ca^{2+} homeostasis using specific organelle-targeted aequorin (AEQ) probes, including those that were targeted to the cytosol (cytAEQ), mitochondria (mtAEQ), and endoplasmic reticulum (erAEQ; Bonora *et al.*, 2013b). Specifically, we cotransfected each aequorin probe with a scrambled oligonucleotide or different concentrations of Mcl-1S3 (Figure 3A). Under all conditions, we investigated the Ca^{2+} response to histamine (His), which signals through Gq-coupled receptors to produce inositol 1,4,5 triphosphate (IP_3; Figure 3A).

Mcl-1S3–expressing cells displayed increased mitochondrial Ca^{2+} uptake after agonist addition (Figure 3A, top). This effect of Mcl-1S3 was dose dependent. We observed a significant increment in $[Ca^{2+}]$ exclusively at the mitochondrial level, which suggested a specific mitochondrial effect (Figure 3A, middle and bottom). Of importance, Mcl-1S3 did not alter the basal mitochondrial Ca^{2+} levels measured by a plasmid encoding the mitochondrial-targeted GCaMP6m (Figure 3B).

These findings indicated that the Mcl-1S3 ASO caused an imbalance in the Mcl-1L/S ratio, which altered mitochondrial Ca^{2+}

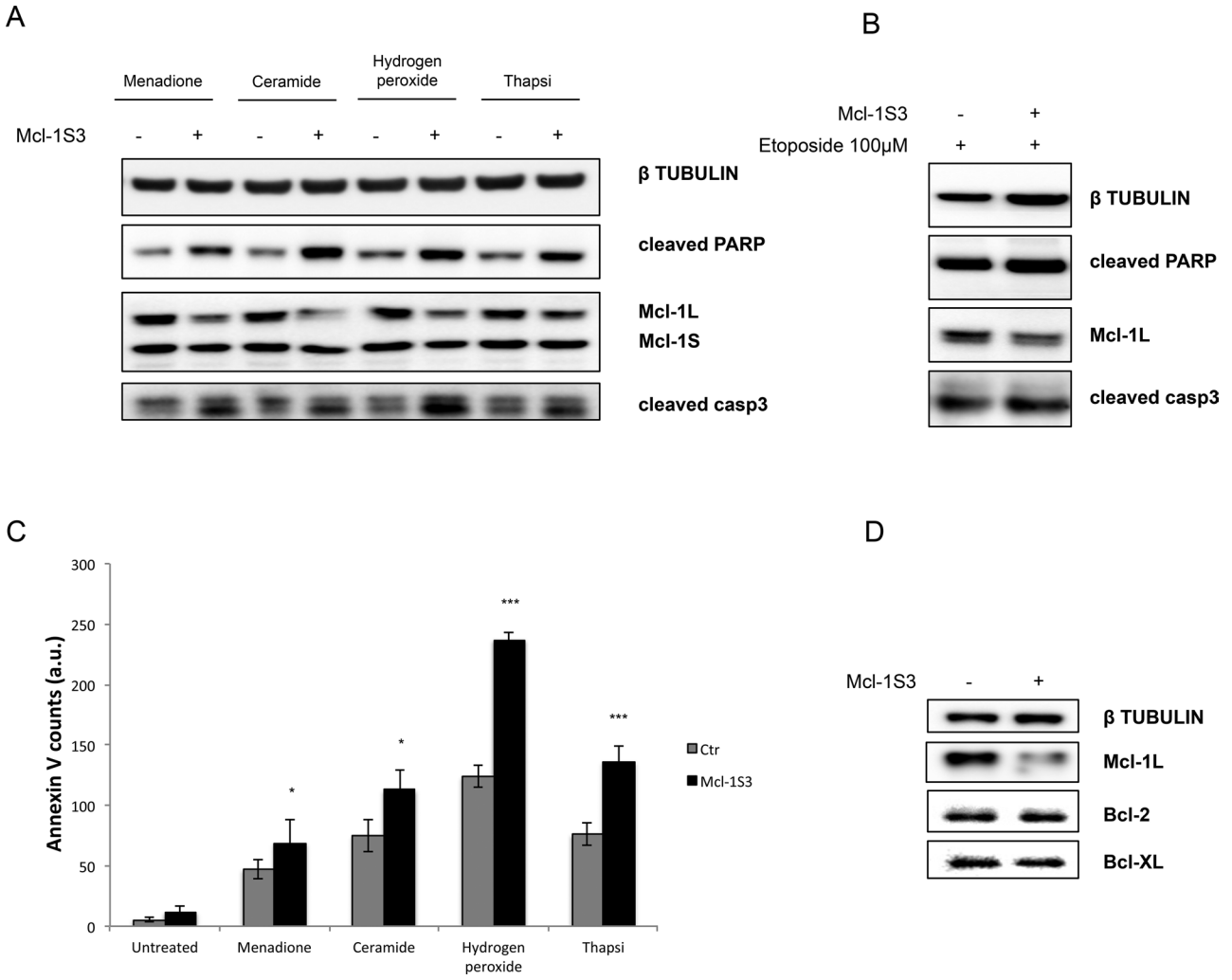

FIGURE 2: Apoptosis in control and experimentally treated HeLa cells. Apoptosis assessment in control and Mcl-1S3-transfected HeLa cells upon treatment with Ca^{2+}-dependent (A) and Ca^{2+}-independent (B) apoptotic stimuli. Western blot analysis of the apoptotic markers cleaved PARP and cleaved caspase 3. (C) Quantification of annexin V–stained cells; significant differences, $*p < 0.05$ and $***p < 0.001$. a.u., arbitrary units. Treatments: 20 μM menadione for 2 h; 10 μM ceramide for 2 h; 1 mM H_2O_2 for 1 h, 4 μM thapsigargin for 2 h; 100 μM etoposide for 3 h. (D) Expression of major antiapoptotic proteins Bcl-2 (26 kDa) and Bcl-XL (26 kDa) upon altering the L/S isoform ratio. $N = 3$ for each experiment.

homeostasis without perturbing other organelles. These data also explained the increased susceptibility to cell death upon the treatment of Mcl-1S3–transfected cells with Ca^{2+}-dependent apoptotic stimuli (as observed in Figure 2, A and C). Of note, pharmacological inhibition of Ca^{2+} uptake with the thiourea derivative KB-R7943 (permeable mitochondrial Ca^{2+} uniporter [MCU] blocker) in Mcl-1S3-transfected cells decreased mitochondrial Ca^{2+} concentration by ~50% (Figure 3C) and protected cells from the ASO-induced effects (Figure 3D). Thus these results suggest that the mitochondrial Ca^{2+} level plays a pivotal role in determining susceptibility to cell death when Mcl-1 levels are unbalanced.

We further explored whether the decrease in the Mcl-1L/S ratio could modify other mitochondrial parameters, such as organelle morphology and membrane potential.

A greater mitochondrial membrane potential promoted Ca^{2+} uptake in Mcl-1S3–treated HeLa cells

The mitochondrial membrane potential Ψ_m is a critical regulator of Ca^{2+} accumulation (Scarpa and Azzone, 1970; Vinogradov and Scarpa, 1973; Gunter and Pfeiffer, 1990; Suski *et al.*, 2012): depolarization reduces the driving force for Ca^{2+} uptake by mitochondria and thereby prevents Ca^{2+} overload. Conversely, hyperpolarization increases Ca^{2+} uptake. To measure $\Delta\Psi_m$ changes, we stained mitochondria with a fluorescent cationic probe, tetramethylrhodamine methyl ester (TMRM), and analyzed the cells by confocal microscopy. To allow for nonspecific TMRM binding, we corrected measurements for residual TMRM fluorescence after full $\Delta\Psi_m$ collapse with the mitochondrial uncoupler carbonyl cyanide 4-(trifluoromethoxy) phenylhydrazone (FCCP).

Mcl-1S3–transfected cells had a significant increase in Ψ_m compared with the controls (Figure 4A). Of importance, the mitochondrial hyperpolarization that was observed upon reduction of the Mcl-1L/S ratio could explain the previously described increase in mitochondrial Ca^{2+} accumulation (Figure 3A).

Subsequently we assessed whether Mcl-1S3 could modify the expression level of the MCU, which facilitates Ca^{2+} uptake into the mitochondrial matrix (Marchi and Pinton, 2014). No difference

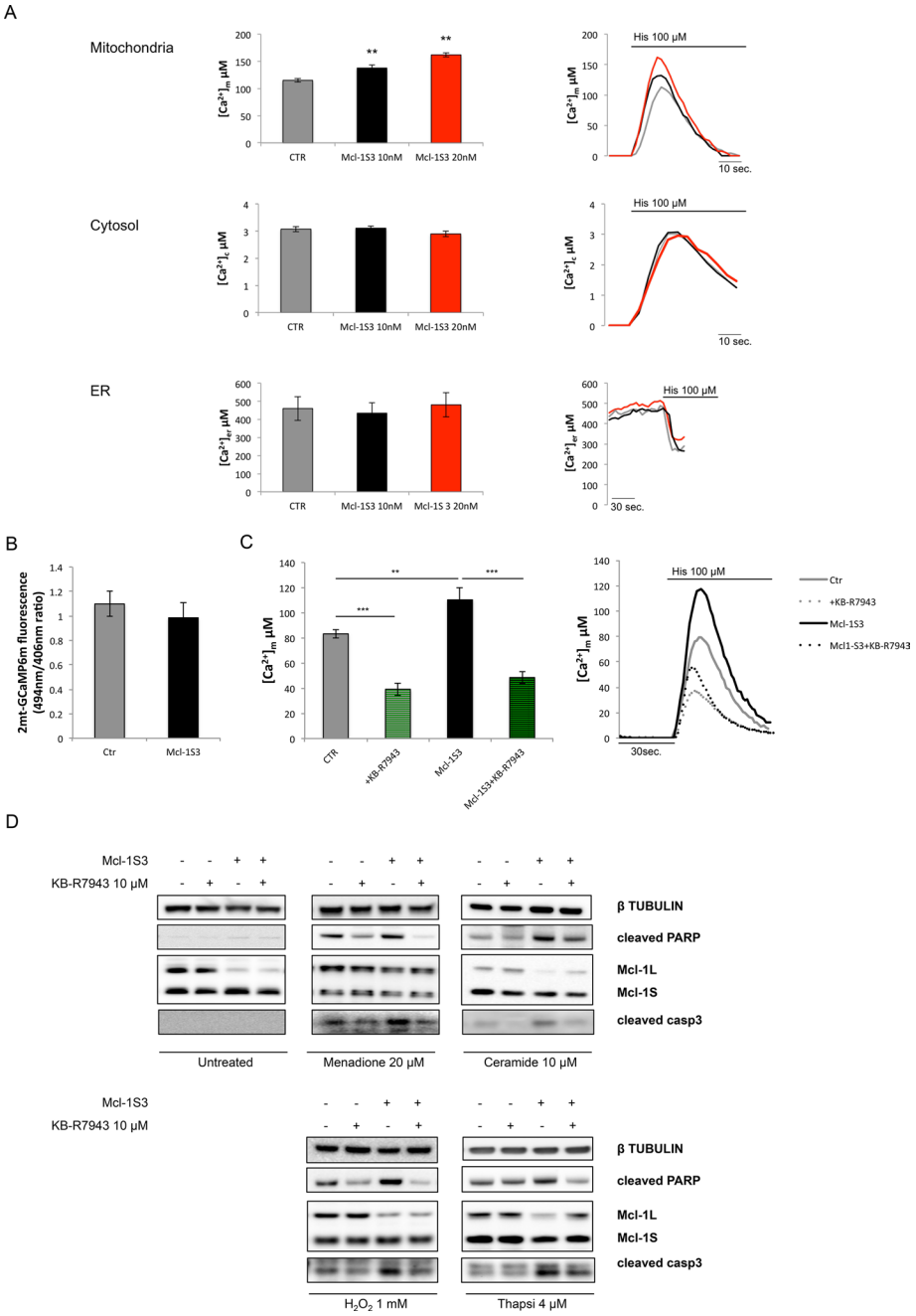

FIGURE 3: Ca^{2+} homeostasis and its role in the death of experimentally treated HeLa cells. (A) Ca^{2+} homeostasis was monitored via aequorin in mitochondria (top), cytosol (middle), and ER (bottom) in control and Mcl-1S3–transfected HeLa cells. The ASO had a specific, dose-dependent mitochondrial effect, as indicated by the black (10 nM Mcl-1S3) and red (20 nM Mcl-1S3) bars. (B) Basal mitochondrial Ca^{2+} concentrations were further assessed by imaging 2mt-GCaMP6m–expressing cells. (C) $[Ca^{2+}]$ upon pharmacological inhibition of mitochondrial Ca^{2+} uptake by the permeable MCU blocker KB-R7943 in control and Mcl-1S3–transfected HeLa cells. KB-R7943 (as confirmed by aequorin measurements) promoted ~50% of the ion concentration in mitochondria. (D) Western blot analysis of the apoptotic markers cleaved PARP and caspase 3 in MCU inhibitor–treated cells. The inhibition of Ca^{2+} uptake protected cells from Ca^{2+}-dependent apoptosis. Where indicated, the cells were challenged with 100 µM histamine. Significant differences, $^{**}p < 0.01$ and $^{***}p < 0.001$. $N = 6$ for each experiment.

in MCU expression was observed upon Mcl-1S3 transfection (Figure 4B). Similarly, the expression levels of other mitochondrial proteins (TIM23 for inner mitochondrial membrane [IMM], ATP5A and HSP60 for matrix, and VDAC and TOM20 for OMM) were also unchanged (Figure 4B; β-tubulin was used as a loading marker). These data suggested that no changes in mitochondrial mass occurred.

Thus variation in Ψ_m appears to be the main cause of increased mitochondrial Ca^{2+} uptake in Mcl-1S3–transfected HeLa cells, which do not exhibit changes in MCU expression, total mitochondrial mass, or mitochondrial biogenesis (as evaluated in Figure 4B by PGC1α detection).

Reduced Mcl-1L/S ratio induced mitochondrial fusion in HeLa cells

Mitochondria are dynamic organelles that fuse and divide to form constantly changing tubular networks (Bereiter-Hahn and Voth, 1994; Scorrano, 2013; Marchi *et al.*, 2014). This evolutionarily conserved activity affects membrane composition (e.g., IMM and OMM) and is mediated by the combined effects of several large GTPases, potentially with other mitochondrial proteins (van der Bliek, 1999).

To assess changes in mitochondrial morphology in our experimental model, we used the mitochondria-targeted red fluorescence protein mtDsRed. Specifically, we cotransfected HeLa cells with either the scrambled oligonucleotide and mtDsRed (control) or Mcl-1S3 and mtDsRed. The fluorescent dye calcein was used as a marker of cell volume to identify living cells and normalize the quantification of the mitochondrial network to cell volume (see *Materials and Methods*).

Confocal images revealed a decreased number of mitochondria in Mcl-1S3–transfected cells (designated as *n° of objects* by the analysis software) compared with the control. Moreover, Mcl-1-S3–transfected cells showed a higher mean mitochondrial volume (Figure 4C). Analyses of the total mitochondrial network and cell volumes revealed no significant differences.

The same results were confirmed in the SH-SY5Y cell line, which displayed a less filamentous network than did HeLa cells (Figure 4D).

Taken together, these findings indicated that 24 h after Mcl-1S3 transfection, a shift from Mcl-1L to Mcl-1S promoted mitochondrial fusion without altering the total mitochondrial volume. Of interest, the increased hyperfusion was not linked to enhanced expression of fusion proteins, such as MFN1/2 and OPA1 (Figure 4E).

These data indicated that shifting from antiapoptotic to proapoptotic Mcl-1 isoforms promoted mitochondrial hyperpolarization and increased mitochondrial fusion in HeLa and SH-SY5Y cells.

A lower Mcl-1L/S ratio induced mitochondrial hyperfusion in a Drp1-dependent manner

In humans, mitochondrial fission is highly regulated by Fis1 and Drp1. Drp1 is a member of the dynamin superfamily of proteins; it consists of a GTPase and a GTPase effector domain and has a predominantly cytosolic localization. Drp1 overexpression induces extensive mitochondrial fragmentation, whereas its depletion promotes fusion (Smirnova *et al.*, 2001). Thus mitochondrial fusion can originate from either lack of fragmentation or up-regulation of fusion proteins.

Accordingly, after excluding a possible role for MFN1/2 and OPA1 proteins, we investigated whether the augmented mitochondrial fusion that was observed upon Mcl-1S3 transfection occurs in a Drp1-dependent manner (Figure 5). To induce mitochondrial fission, we overexpressed wild-type Drp1. Drp1 overexpression promoted mitochondrial fission (Figure 5A, bottom, white bars with gray stripes), which was quantitatively expressed as an increased number of mitochondrial objects and a reduction of the mean volume of a single mitochondrial object. Surprisingly, cotransfection of Mcl-1S3 and Drp1 abolished the fragmentation of the mitochondrial network, reestablishing a mitochondrial shape that resembled the control condition.

These data suggested that Drp1 and Mcl-1 are functionally related in the regulation of mitochondrial morphology through a balance between fusion and fission events.

Inhibiting Drp1 activity in the mitochondria promoted apoptotic cell death

To investigate the link between cell death and Drp1/Mcl-1L–driven changes in morphology in our experimental model, we monitored the activation of apoptosis in control and Mcl-1S3–transfected HeLa cells by WB analysis. We subjected these cells to forced fission (by the transfection of wild-type Drp1) and then treated them with apoptotic Ca^{2+}-dependent and Ca^{2+}-independent stimuli as previously described.

As in Figure 2, there was a higher percentage of apoptotic cells after Mcl-1S3 transfection than with the control upon Ca^{2+}-dependent treatments, whereas no apoptosis was detected for any of the conditions lacking apoptotic stimuli (Figure 6A). Of note, fragmentation of the mitochondrial network of control cells by Drp1 overexpression provided protection from cell death, whereas apoptosis occurred at levels between those of the control and ASO groups when fission was inhibited by down-regulation of Mcl-1L (Figure 6A, lane Mcl-1S3+Drp1). In all conditions concerning down-regulation of Mcl-1L and experimental treatments, no significant changes in Mcl-1S expression were detected. These observations were not seen with etoposide treatment.

In contrast, when the functionality of Drp1 was abolished by the use of its dominant-negative Drp1-K38A, cells with a persistent mitochondrial hyperfusion state (Yoon *et al.*, 2001) died, based on PARP and caspase 3 cleavage (Figure 6B).

These final experiments indicated a strong link between changes in mitochondrial morphology driven by Mcl-1L and Drp1 and the intrinsic apoptotic pathway previously described.

Mcl-1: a link between cell cycle and mitochondrial dynamics

In a study focused on the link between mitochondrial morphology and cell cycle progression, Mitra *et al.* (2009) described a greater membrane potential and a massive, hyperfused network state in mitochondria at the G_1/S transition of the cell cycle. In light of our previous observations of Mcl-1 ASO transfection, which echoed their findings, we proceeded to investigate the Mcl-1 expression pattern at the G_1/S transition after the cells were synchronized with a double- thymidine block. Of interest, we observed a shift in the Mcl-1L/S ratio at the G_1/S transition, with a greater amount of Mcl-1S than Mcl-1L (Figure 7).

Drp1 interacted with Mcl-1L to regulate mitochondrial dynamics

Next, to further support our model, we investigated whether Drp1 could be coimmunoprecipitated with Mcl-1L. As shown in Figure 8A, Mcl-1L formed immune complexes with Drp1 in control HeLa cells, whereas Mcl-1S remained in the supernatant. The same result was obtained by performing the experiment in reverse; immunoprecipitation of overexpressed Drp1 and antibody cross-linking to protein A agarose revealed a preferential binding to Mcl-1L. These data suggested that the two proteins specifically interacted with each other to regulate the hyperfused mitochondrial state detected in previous experiments.

Lowering the Mcl-1L/S ratio inhibited Drp1 translocation from the cytosol to mitochondria

Drp1 localizes primarily in the soluble fraction of the cell (Shin *et al.*, 1997). Although Drp1 can be found in membrane compartments, membrane localization occurs only under certain environmental conditions and depends on the phase of the cell cycle (Smirnova *et al.*, 2001).

In HeLa cells, we detected Drp1 predominantly in the cytosol, which is in agreement with current literature, and moderately at the mitochondrial membranes (Figure 8B), where it likely exerts physiological roles in maintaining a basal fission rate. In contrast, Mcl-1L was enriched at the mitochondria, whereas Mcl-1S was found in the cytosol and endoplasmic reticulum (ER) compartments.

Drp1 translocates from the cytosol to mitochondria to exert its profission functions. To evaluate Mcl-1L function at the OMM during the fission/fusion processes, we assessed the amount of mitochondrial Drp1 after overexpressing Drp1 and after altering the Mcl-1L/S ratio. As shown in Figure 8C, upon Drp1 overexpression, the level of mitochondrial Drp1 increased compared with mock-transfected cells. On Mcl-1S3 transfection, which consequently depleted Mcl-1L, Drp1 accumulation at mitochondria was less efficient (Figure 8C).

These findings suggested that Mcl-1L acts as a molecular anchor for mitochondrial Drp1 and further validated the pivotal role of Mcl-1L/S balance in the regulation of the fusion and fission machinery.

DISCUSSION

Dysregulation of apoptosis contributes to numerous pathological conditions, including cancer. Indeed, one of the hallmarks of cancer cells is their capacity to evade apoptosis, prompting research for drugs that can restore cell death susceptibility in tumor cells (Fesik, 2005). The mitochondrial apoptotic pathway is regulated by interactions between members of the Bcl-2 protein family, which contain up to four BH domains (BH1–4; Kuwana and Newmeyer, 2003; Hardwick and Youle, 2009; Akl *et al.*, 2014). Protein factors possessing all four BH domains, including Mcl-1L, antagonize apoptosis by preventing mitochondrial outer membrane permeabilization (MOMP), thus sequestering proapoptotic factors in mitochondria. Factors lacking one or more BH domains, including Mcl-1S, are proapoptotic and promote MOMP. Mcl-1L is highly expressed in human malignancies, and its cellular localization is consistent with a role in controlling key mitochondrial events during apoptosis (Thomas *et al.*, 2010).

Mitochondrial Ca^{2+} also plays a critical role in the regulation of cell death (Hajnoczky *et al.*, 2006; Giorgi *et al.*, 2012; Rimessi *et al.*, 2015). Two requisite events during the early stages of apoptosis are the ER

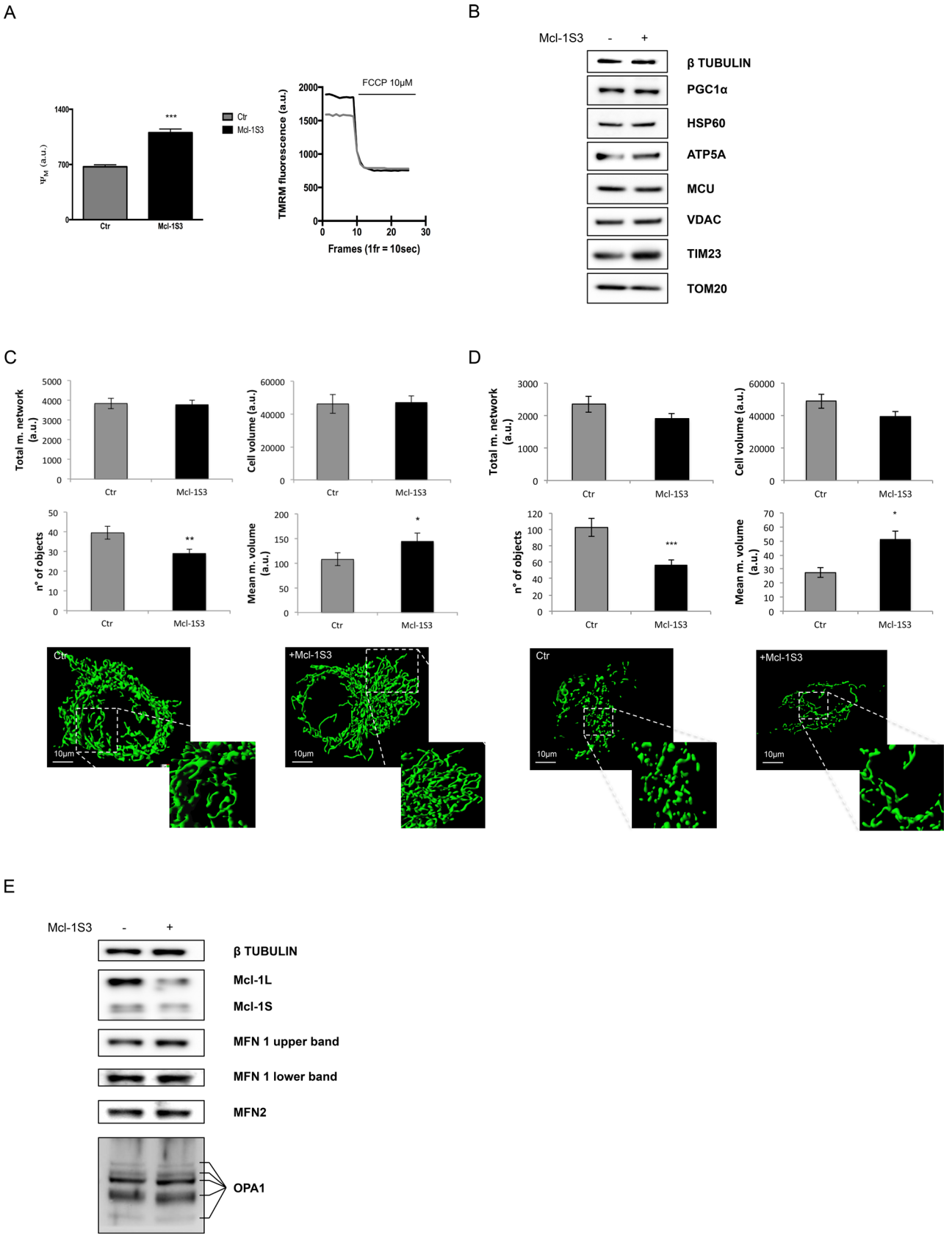

FIGURE 4: The Ψ_m and morphological changes in the mitochondria of ASO-transfected HeLa cells. (A) Mcl-1S3-treated HeLa cells had a greater mitochondrial membrane potential than the untreated cells. (B) Western blot analysis to monitor changes in the expression of proteins involved in Ca^{2+} uptake (MCU), mitochondrial mass (HSP60, ATP5A, VDAC, TIM23, TOM20), and biogenesis (PGC1α). (C, D) Parameters describing the mitochondrial network dynamics

release of Ca^{2+} into the cytosol and the mitochondrial release of cytochrome *c*. The Ca^{2+} uptake by the mitochondria determines cell susceptibility to apoptotic stimuli. For example, reduced ER Ca^{2+} flux toward mitochondria results in resistance to apoptosis (Pinton *et al.*, 2011; Marchi *et al.*, 2012, 2013; Bononi *et al.*, 2013; Giorgi *et al.*, 2015; Patergnani *et al.*, 2015), inhibiting the mitochondrial Ca^{2+} overload required for permeability transition pore opening (Bonora *et al.*, 2013a).

Several earlier studies described the role of Mcl-1 in Ca^{2+} homeostasis. Minagawa *et al.* (2005) showed that Mcl-1 overexpression did not affect IP_3 receptor (IP_3R) expression or the amount of Ca^{2+} contained in ER stores. However, mitochondrial Ca^{2+} signals were decreased in cells overexpressing Mcl-1

Conversely, Eckenrode *et al.* (2010) proposed a different activity for Mcl-1 that is quite similar to the molecular mechanism of Bcl-2 function. They reported that Mcl-1 bound with comparable affinity to the C-ter of different IP_3R isoforms, with the cells consequently displaying low ER Ca^{2+} content and an enhanced rate of IP_3-mediated Ca^{2+} release. Moreover, Mcl-1 expression enhanced spontaneous IP_3R-dependent Ca^{2+} oscillations and spiking in intact cells in the absence of agonist stimulation.

The data presented here support a mitochondria-specific function for Mcl-1, with no effect on ER Ca^{2+} homeostasis (Figure 3A). In contrast to previous studies (Varadarajan *et al.*, 2013), we used an antisense oligonucleotide approach to modulate mRNA splicing rather than direct overexpression, silencing, or antagonism of the protein to investigate Mcl-1 functional features.

Because of the high therapeutic potential of ASOs, especially in combination with cytotoxic agents (Wacheck *et al.*, 2006; Skoda *et al.*, 2008), we opted for splice-switching antisense technology to modulate the balance between the different variants of Mcl-1. To guarantee high gene specificity for Mcl-1 pre-mRNA and reduce potential off-target toxic effects, we designed a novel Mcl-1S3 sc-ASO that targets an ESE within exon 2 (Figure 1D) and were able to successfully induce exon skipping, which permitted an appreciable and dose-dependent increase in Mcl-1S expression (Figure 1E). Of most importance, this effect was associated with an extensive induction of cell death through the mitochondrial intrinsic apoptotic pathway (Figure 2), which further supports the role of Mcl-1 pre-mRNA AS as a target for the development of anticancer therapies. It is worth noting that intervention at the pre-mRNA level would maintain the transcriptional regulation and absolute levels of Mcl-1 pre-mRNA, thus selectively decreasing the long/short isoform ratio, which has proapoptotic effects. In cells overexpressing the Mcl-1L pre-mRNA in a manner similar to tumors, the splice-switching strategy would result in a marked increase in the Mcl-1S form, thus magnifying the proapoptotic effect compared with the generic silencing of Mcl-1L expression.

Using Mcl-1S3, we showed that the shift in the Mcl-1L/S ratio resulted in increased mitochondrial Ca^{2+} levels after agonist addition without affecting its baseline content (Figure 3B) or the Ca^{2+} homeostasis of other subcellular organelles. These data suggest that the lower Mcl-1L/S ratio affects mitochondrial Ca^{2+} uptake only when the cytosolic [Ca^{2+}] rapidly increases (i.e., upon Ca^{2+}-dependent apoptotic stimuli).

Under our experimental conditions, the higher mitochondrial Ca^{2+} uptake observed on Mcl-1S3 transfection was certainly due to a significant increment in the mitochondrial membrane potential (Figure 4A). Variation in $\Delta\Psi_m$ is a highly sensitive indicator of the energetic state of mitochondria and is strictly associated with the morphology of the mitochondrial network.

Of interest, when mitochondrial potential was monitored at different cell cycle stages, it appeared to be the greatest at G_1/S. Nevertheless, mitochondria form a giant tubular network in G_1/S (Mitra *et al.*, 2009). Accordingly, we observed a shift in the Mcl-1L/S ratio during G_1/S phase, with a greater amount of Mcl-1S present compared with the L variant (Figure 7). A higher level of Mcl-1L was detected at G_0, which coincides with greater mitochondrial fragmentation (Mitra *et al.*, 2009). Moreover, we also detected a low Mcl-1L/S ratio during mitosis, which is characterized by a high number of tubular mitochondria.

These findings suggest a pivotal role of Mcl-1 in the regulation of the fusion and fission dynamics, which occurs in a Drp1-dependent manner. Mcl-1 interacts with Drp1 (Figure 8A). On Mcl-1S3 transfection, Drp1 was unable to induce extensive fragmentation (Figure 5). This finding suggests that the reduction of Mcl-1L at the OMM may prevent the normal physiologic functions of Drp1, producing a persistent hyperfused mitochondrial state (Figure 4, C and D) without changes in fusion protein expression (Figure 4E).

Recently a pivotal role for Mcl-1 in regulating fusion/fission dynamics was proposed (Perciavalle *et al.*, 2012; Varadarajan *et al.*, 2013), based on extensive mitochondrial fragmentation upon Mcl-1 down-regulation, which occurred independently of Mcl-1–related apoptosis. These studies used either *Mcl-1* deficient MEFs (Perciavalle *et al.*, 2012) or pharmacological inhibition (BH3 mimetics) of Mcl-1 expression (Varadarajan *et al.*, 2013). Conversely, our approach was to decrease the Mcl-1L/S ratio, resulting in a hyperfused mitochondrial network and increased sensitivity to apoptosis. Thus, if the inefficient mitochondrial fusion caused by total Mcl-1 inhibition/depletion is not related to altered susceptibility to cell death, the hyperfused state induced by decreasing the Mcl-1L/S ratio might represent a crucial event for sensitizing mitochondria to a wide range of apoptotic stimuli. Of note, we observed a reduced level of mitochondrial Drp1 upon Mcl-1S3 transfection (Figure 8C) without any modification in the total endogenous Drp1 level. These data suggested the putative involvement of the fission factor in Mcl-1–dependent mitochondria remodeling, most likely by regulating Drp1 translocation from the cytosol to the OMM. We also observed the interaction between Drp1 and Mcl-1, although Drp1 overexpression was required. Of interest, Drp1 seems to coimmunoprecipitate with the long form of Mcl-1, but further work is required to clarify the exact relationship between Mcl-1 and Drp1 shuttling/localization.

Another key conclusion from the present study is the link between mitochondrial morphology and apoptosis. Despite the large quantity of literature available on the topic, the relationship between the two events has not been fully elucidated. In particular, Drp1 is described as both a fundamental inducer of apoptosis

shown in histograms (top) and confocal images (bottom). Black bars indicate Mcl-1S3–transfected HeLa (C) and SH-SY5Y (D) cells; a decrease in number of objects and an increase in mean mitochondrial volume are evidence of hyperfused mitochondria. Significant differences, $*p < 0.05$, $**p < 0.01$, and $***p < 0.001$. a.u., arbitrary units. (E) Mitochondrial fusion proteins were investigated by Western blot with MFN1/2 and OPA1 antibodies in both experimental conditions. $N = 3$ for each experiment.

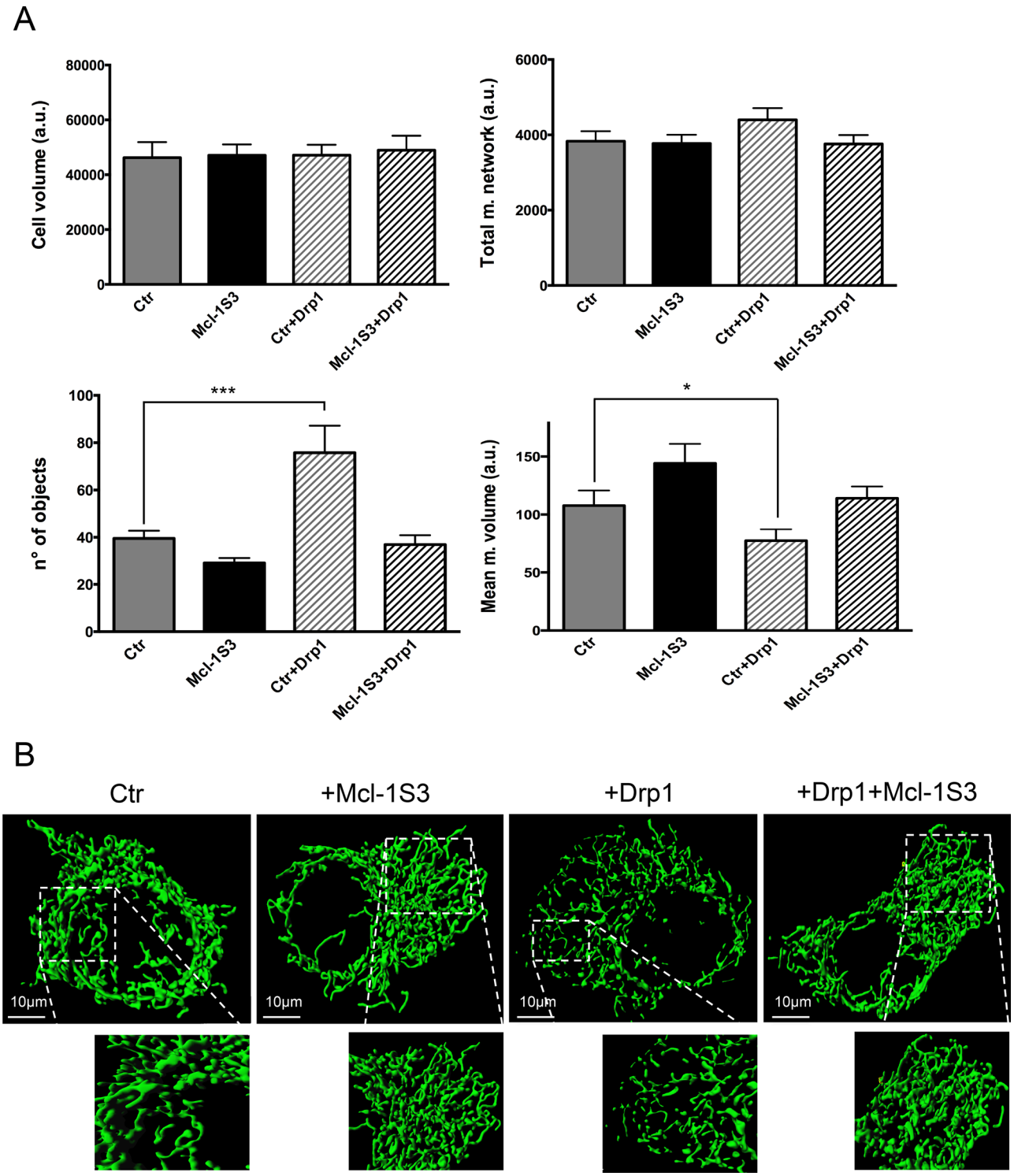

FIGURE 5: Mcl-1L involvement in mitochondrial dynamics is Drp1 dependent. (A) Analysis of mitochondrial morphology under four experimental conditions. No significant differences were detected in cell volume or total mitochondrial network (top). Drp1 overexpression promoted extensive fragmentation, as shown by the increased number of objects and the reduction of mean mitochondrial volume (bottom, white bars with gray stripes). Cotransfection of Mcl-1S3 and Drp1 reversed the effect of Drp1 overexpression alone, suggesting an association between Mcl-1L and Drp1 in the regulation of mitochondrial dynamics. Significant differences, $*p < 0.05$ and $***p < 0.001$. a.u., arbitrary units. (B) Representative confocal images of mitochondrial networks (green fluorescence) under each condition. $N = 3$ for each experiment.

(Frank *et al.*, 2001) and an inhibitor of Ca^{2+}-dependent apoptosis (Szabadkai *et al.*, 2004). The model presented here is more consistent with the latter functionality (Szabadkai *et al.*, 2004), and our findings are further supported by a recent study (Westrate *et al.*, 2014) showing that persistent mitochondrial fusion leads to robust caspase-dependent cell death.

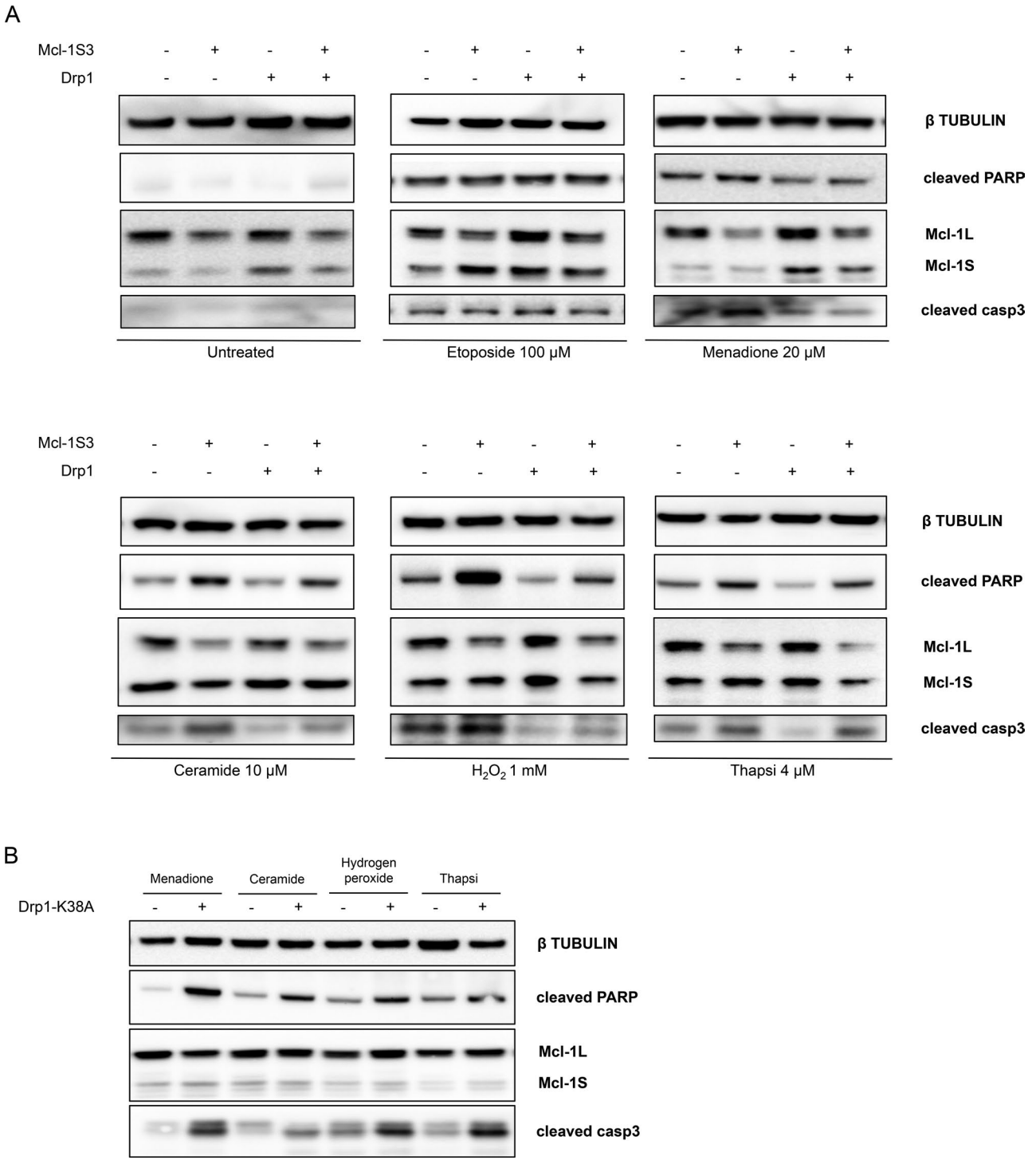

FIGURE 6: Inhibition of Drp1 activity in the mitochondria restored apoptotic cell death. (A) Apoptosis assessment upon treatment with Ca^{2+}-dependent and Ca^{2+}-independent apoptotic stimuli detected by Western blot analysis of cleaved PARP and cleaved caspase 3. Control and Mcl-1S3-transfected HeLa cells were first cotransfected with a wt Drp1 construct (as described in morphology experiments) and then divided into six conditions: untreated (with culture medium exchange), 100 μM etoposide for 3 h, 20 μM menadione for 2 h, 10 μM ceramide for 2 h, 1 mM hydrogen peroxide for 1 h, and 4 μM thapsigargin for 2 h. (B) Overexpression of the dominant-negative Drp1-K38A promotes mitochondrial fusion and widespread cell death. $N = 3$ for each experiment.

In contrast to the current opinion that mitochondrial fragmentation is associated with apoptosis, our data indicate that apoptosis can also occur when mitochondria are hyperfused, as shown in Figure 6A, upon the inhibition of Drp1 activity in the mitochondria by Mcl-1S3 transfection and as shown with regard to BAX-dependent MOMP failure when mitochondria are fragmented (Renault *et al.*, 2014). The same effect was also confirmed with the dominant-negative form Drp1-K38A (Yoon *et al.*, 2001) in all experimental

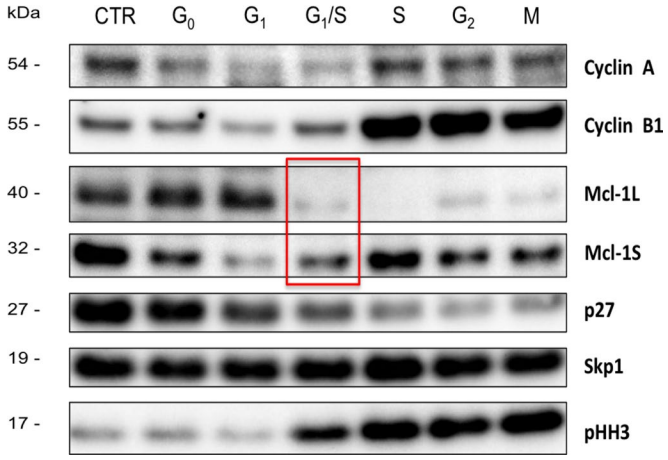

FIGURE 7: Mcl-1 links cell cycle regulation and mitochondrial dynamics. Mcl-1L and Mcl-1S expression levels are shown in different phases of the T98G cell cycle. Cells were synchronized by double-thymidine block and assayed at each phase of the cell cycle (top). Proteins of interest are shown on the right. Skp1 was used as a loading control. Other markers: cyclin A for S and M phases; cyclin B for the G_2/M checkpoint; p27 for quiescent cells; and pHH3 for mitotic activity. The red rectangle indicates Mcl-1L and Mcl-1S expression in G_1/S phase. $N = 2$.

conditions (Figure 6B). An intact mitochondrial network could ensure rapid propagation of Ca^{2+} through the mitochondrial matrix to promptly trigger apoptosis. Of note, we obtained a similar result when Mcl-1L was down-regulated by Mcl-1S3, thus avoiding Drp1 activity at the OMM. However, if Drp1 is free to act at the mitochondria, fragmentation could inhibit the propagation of the apoptotic wave, limiting the harmful effects caused by treatment.

In this scenario, Ca^{2+} signaling behaves as the primary initiator of cell death, and accordingly, the pharmacological inhibition of MCU by KB-R7943 (Figure 3C) protected cells from the therapeutic effects of Mcl-1S3 (Figure 3D).

Taken together, these data suggest that redirecting Mcl-1 synthesis from the antiapoptotic L variant to the proapoptotic S variant might represent a novel strategy for anticancer therapies.

MATERIALS AND METHODS

Reagents and solutions

All reagents were purchased from Sigma-Aldrich (St. Louis, MO), Thermo Scientific (Waltham, MA), and Santa Cruz Biotechnology (Dallas, TX).

Cell culture and transient transfection

HeLa cells were grown in DMEM and SH-SY5Y cells in RPMI 1640, both supplemented with 10% fetal bovine serum (FBS), in 75-cm^2

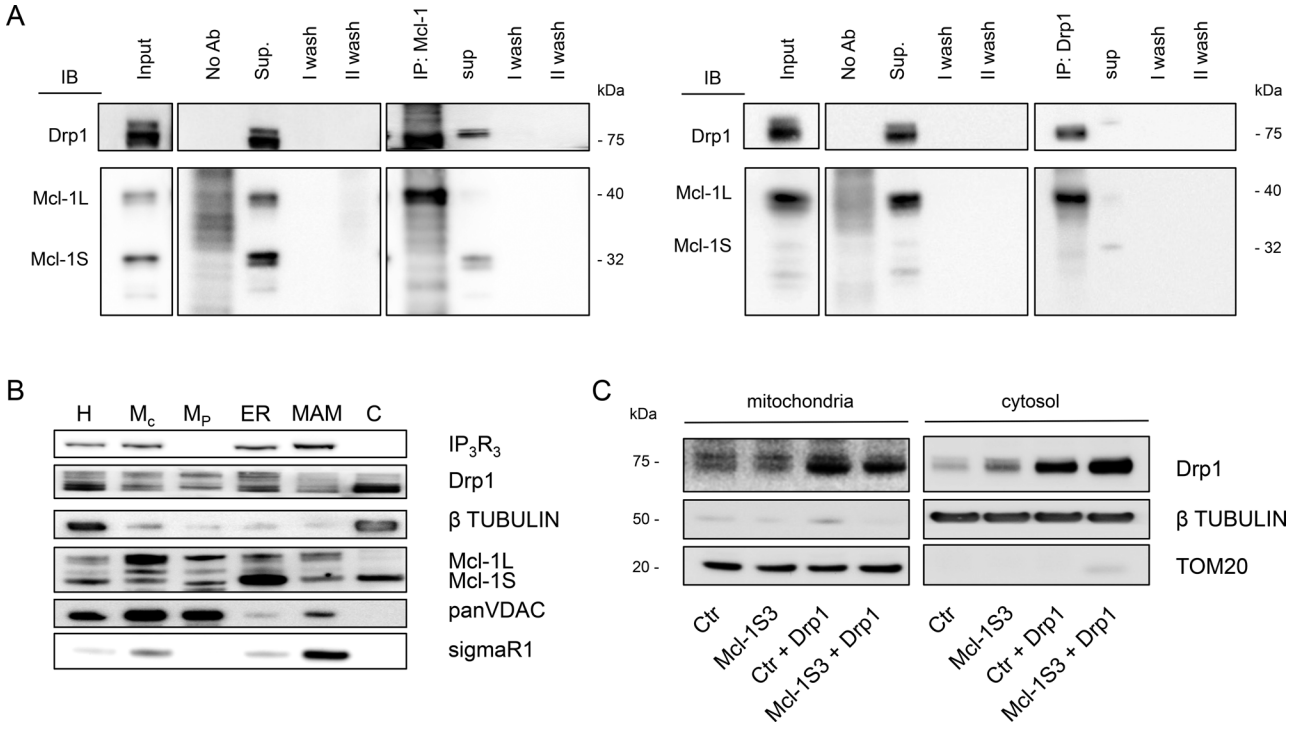

FIGURE 8: Subcellular localization of Drp1, Mcl-1L/Mcl-1S, and their interactions. Coimmunoprecipitation of Mcl-1L and Drp1 in HeLa cells. (A) Immunoprecipitation (IP) was performed in control (in absence of antibody), with rabbit anti–Mcl-1 antibody, and in a reverse IP mode with rabbit anti-Drp1 antibody followed by immunoblotting with anti–Mcl-1 and anti-Drp1 antibodies. Input lysates as well as flowthrough after the IPs are shown. (B) Subcellular localization of Drp1, Mcl-1L, and Mcl-1S as determined by fine fractionation. IP_3R_3, β-tubulin, panVDAC, and sigmaR1 were used as markers of ER, cytosol, mitochondria, and MAM, respectively. H, homogenate; M_c, crude mitochondria; M_P, pure mitochondria; ER, endoplasmic reticulum; MAM, mitochondria-associated membranes; C, cytosol. (C) Induction of Drp1 translocation from cytosol to mitochondria upon Drp1 overexpression in control and Mcl-1S3–transfected cells. Protein localization and expression were evaluated under each condition by WB after digitonin-based fractionation. $N = 3$ (for each experiment).

Corning flasks. All cells were maintained at 37°C and 90% relative humidity in 5% CO_2. Before transfection, cells were seeded onto 13-mm glass coverslips for intracellular Ca^{2+} measurements and onto 24-mm glass coverslips for microscopic analysis. Next plasmid transfections (see later description) with Lipofectamine 2000 were performed. All experiments were performed 24 h after transfection.

In experiments involving KB-R7943, for Ca^{2+} measurements and apoptosis, cells were pretreated for 15 min with 10 µM KB-R7943 in complete medium.

Primers for RT-PCR

Oligonucleotides for RT-PCR were created online (Primer3) using the human Mcl-1 sequence from the National Center for Biotechnology Information database as a template. The primer sequences are as follows: forward (5′-3′), GAGGAGGAGGAGGACGAGTT (Mcl-1 Ex1F1); reverse (5′-3′), TCCTCTTGCCACTTGCTTTT (Mcl-1 Ex3r1).

All PCR products were separated by 2% agarose gel electrophoresis and visualized with ethidium bromide. The expected sizes were 689 base pairs for Mcl-1L and 441 base pairs for Mcl-1S.

mRNA splicing pattern and protein expression of Mcl-1

HeLa cells were plated onto 35-mm plates. After transfection, total RNA was extracted using the phenol/chloroform method. All steps were performed at 4°C. RNA was quantified with a NanoDrop ND-1000, and protein/solvent contaminations were evaluated ($A_{260/280}$ = 1.8 and $A_{260/230}$ = 2.0). RNA was converted to cDNA and amplified using the Mcl-1 primers via RT-PCR (SuperScript III one-step RT-PCR system with Platinum Taq DNA polymerase; Invitrogen).

Proteins were separated by SDS–PAGE on a 4–12% precast gel and detected by Western blotting using polyclonal rabbit anti-Mcl-1 (1:500) for both the L (40 kDa) and S (32 kDa) isoforms (Santa Cruz Biotechnology) and monoclonal mouse anti–β-tubulin (1:5000; Sigma-Aldrich) as the primary antibodies and respective horseradish peroxidase (HRP)–labeled secondary antibodies (1:5000), according to standard protocols.

Inhibition of proteasomal degradation

HeLa cells were plated onto 35-mm-well plates for a time-lapse experiment. Twenty-four hours after plating, cells were treated with 10 µM MG132 (dissolved in dimethyl sulfoxide [DMSO]) for 3, 6, 9, and 12 h. The control cells were treated with DMSO alone. Mcl-1 expression was then detected by Western blotting as described previously.

Design of ASOs

ASOs were synthesized in collaboration with Daniela Perrone and coworkers at the Department of Chemical and Pharmaceutical Sciences, University of Ferrara (Ferrara, Italy). The putative ESE in Mcl-1 exon 2 was identified using ESEfinder (rulai.cshl.edu/tools/ESE2/), and the secondary structures of the sc-ASOs were analyzed using Sfold (sfold.wadsworth.org/cgi-bin/index.pl). The sc-ASOs were designed and then chemically synthesized to contain 2′-O-methyl–modified RNA and a full-length phosphorothioate backbone.

The oligonucleotide sequences were as follows: Mcl-1S3 (5′-3′), AACGUCUGUGAUACUUUCUGCUAAU; and scramble (5′-3′), AUUAUGCUUUUGACCCGAUUAAUCG.

Apoptosis assessment

For WB, HeLa cells were plated onto 35-mm-well plates. After transfection of ASOs and treatment with Ca^{2+}-dependent (20 µM menadione for 2 h; 10 µM ceramide for 2 h; 1 mM H_2O_2 for 1 h, 4 µM thapsigargin for 2 h) or Ca^{2+}-independent (100 µM etoposide for 3 h) apoptotic stimuli, cells were trypsinized, pelleted (1100 rpm, 5 min, +4°C), resuspended, and homogenized (EBC buffer with protease/phosphatase inhibitor cocktail, pH 7.4). Proteins were separated by SDS–PAGE on a 4–12% precast gel, and the levels of cleaved PARP (89 kDa), β-tubulin (50 kDa), and cleaved caspase 3 (17 kDa) were estimated by WB using polyclonal rabbit anti-PARP (1:1000), polyclonal rabbit anti-caspase 3 (1:1000), and monoclonal mouse anti–β-tubulin (1:5000) primary antibodies according to standard protocols. Antibodies were purchased from Cell Signaling and Sigma-Aldrich. Nitrocellulose membranes were incubated with appropriate HRP-conjugated secondary antibodies (1:5000; Santa Cruz Biotechnology), and protein bands were then visualized by chemiluminescence.

For annexin V staining, HeLa cells were plated onto 35-mm-well plates. After transfection of ASOs and treatment with Ca^{2+}-dependent apoptotic stimuli, cells were gently harvested, processed with buffers, and incubated with annexin V according to manufacturer's protocols (BioVision). The green fluorescence signal was quantified under all conditions on a Tali image-based cytometer.

Aequorin measurement

For cytAEQ and mtAEQmut at 24 h posttransfection, the coverslips were incubated with 5 µM coelenterazine for 1.5 h in Krebs–Ringer modified buffer (KRB; 125 mM NaCl, 5 mM KCl, 1 mM Na_3PO_4, 1 mM $MgSO_4$, 5.5 mM glucose, and 20 mM 4-(2-hydroxyethyl)-1-piperazineethanesulfonic acid [HEPES], pH 7.4, at 37°C) supplemented with 1 mM $CaCl_2$. To reconstitute erAEQ with high efficiency, the luminal [Ca^{2+}] of the ER was first reduced by incubating the cells for 45 min at 4°C in KRB supplemented with 5 µM coelenterazine, the Ca^{2+} ionophore ionomycin, and 600 µM ethylene glycol tetraacetic acid (EGTA). After incubation, the cells were extensively washed with KRB supplemented with 2% bovine serum albumin and 2 mM EGTA before the luminescence measurement was initiated. Aequorin signals were measured in KRB supplemented with either 1 mM $CaCl_2$ or 100 µM EGTA, using a purpose-built luminometer. The agonist (histamine at 100 µM) was added to the same medium. The experiments were terminated by lysing the cells with Triton X-100 in a hypotonic Ca^{2+}-rich solution (10 mM $CaCl_2$ in H_2O), thus discharging the remaining aequorin pool. The light signals were collected and calibrated with [Ca^{2+}] values. Further experimental details were previously described (Bonora *et al.*, 2013b).

Mitochondrial Ca^{2+} concentration measurements with 2mt-GCaMP6m

To test resting mitochondrial Ca^{2+} concentrations with high sensitivity, we used a new Ca^{2+} probe based on the last-generation GCaMP probe (Chen *et al.*, 2013) targeted to the mitochondrial matrix. We chose the GCaMP6m version because it had the highest Ca^{2+} affinity. To measure the signal independent of variations in basal fluorescence intensity due to the variable expression levels of the probe, we took advantage of the isosbestic point in the GCaMP6m excitation spectrum; exciting GCaMP6m at 406 nm led to fluorescence emission that was not Ca^{2+} dependent. As a consequence, the ratio between the excitation wavelengths of 494 and 406 nm was proportional to the Ca^{2+} concentration and independent of probe expression levels. Cells were imaged with an IX-81 automated epifluorescence microscope (Olympus) equipped with a 40× oil immersion objective (numerical aperture 1.35; Olympus) and an ORCA-R2 charge-coupled device camera (Hamamatsu Photonics).

Microscopic analysis

Mitochondrial morphology was assessed under four conditions: control, Mcl-1S3, control plus Drp1, and Mcl-1S3 plus Drp1. Under

each condition, cells were transfected with 1 μg of mtDSred (excitation/emission: 556/586 nm) and stained with 1 μM calcein (excitation/emission: 495/515 cm) for 10 min at 37°C to mark the mitochondria and to normalize for cell volume.

The Ψ_m was assessed under two conditions: control and Mcl-1S3. Under each condition, cells were incubated with 10 nM TMRM (excitation/emission: 548/573 nm) for 20 min at 37°C. Steady-state and poststimulation (FCCP 10 μM) dye intensities were quantified.

All of the experiments were performed on a confocal Nikon Eclipse T_i system. Fluorescent images were captured and analyzed using NisElements 3.2 for membrane potential and Imaris 4.0 software for morphology. To improve image resolution, *Z*-series acquisitions were deconvolved using Huygens Essential 3.3 software.

Mitochondrial mass and biogenesis

Control and Mcl-1S3–transfected HeLa cells were harvested, washed, and pelleted (1100 rpm, 5 min, +4°C) in phosphate-buffered saline (PBS), resuspended in RIPA buffer supplemented with protease and phosphatase inhibitor cocktail (pH 7.4), and homogenized. After measurement of the concentrations, proteins were separated by SDS–PAGE on a 4–12% precast gel, and the levels of two protein markers for each mitochondrial compartment were detected using the primary antibodies rabbit anti-VDAC (1:2500, 31 kDa) and anti-TOM20 (1:5000, 20 kDa) for OMM, rabbit anti-MCU (1:2000, 35 kDa) and mouse anti-TIM23 (1:5000, 23 kDa) for IMM, and mouse anti-HSP60 (1:5000, 60 kDa) and anti-ATP5A (1:5000, 55 kDa) for matrix. Anti–β-tubulin (1:5000, 50 kDa) was included as a loading control. After overnight incubation, the nitrocellulose membranes were incubated with appropriate HRP-conjugated secondary antibodies (1:5000; Santa Cruz Biotechnology), and the proteins were visualized by chemiluminescence. Similarly, for the evaluation of biogenesis, anti-PGC1α antibody (1:1000, 113 kDa) was used. The expression of fusion proteins was detected by anti-MFN1 (1:1000, 60 and 86 kDa), anti-MFN2 (1:1000, 90 kDa), and anti-OPA1 (1:1000, 88 and 93 kDa for major isoforms).

Cell cycle synchronization

T98G cells were synchronized using a double-thymidine block. Briefly, T98G cells in a 100 × 20 mm Petri dish were treated with 2 mM thymidine (Sigma-Aldrich) for 16 h. The cells were washed once in fresh medium to remove the thymidine and then incubated in fresh complete medium. After 6 h, 2 mM thymidine was added again, and the cells were incubated for an additional 16 h. After the second thymidine treatment, the cells were washed and resuspended in fresh complete medium. Cell cycle progression was studied at 2-h intervals using phase-specific markers: cyclin A for the S and M phases; cyclin B for the G_2/M checkpoint; p27 for the G_0 cells; and pHH3 for mitotic activity. Skp1 was used as a loading control.

Subcellular fractionation

Cell fractionation was performed using HeLa cells as described (Wieckowski *et al.*, 2009). Cells (10^9) were harvested, washed with PBS (supplemented with 2 mM Na_3VO_4 and 2 mM NaF when the preservation of protein phosphorylation states was required) by centrifugation at 500 × *g* for 5 min, resuspended in homogenization buffer (225 mM mannitol, 75 mM sucrose, 30 mM Tris-HCl, pH 7.4, 0.1 mM EGTA, and phenylmethylsulfonyl fluoride), and gently disrupted by Dounce homogenization. The homogenate was centrifuged twice at 600 × *g* for 5 min to remove nuclei and unbroken cells, and the supernatant was then centrifuged at 10,300 × *g* for 10 min to pellet crude mitochondria. The resultant supernatant was centrifuged at 20,000 × *g* for 30 min at 4°C. This pellet consisted of the lysosomal and plasma membrane fractions. Further centrifugation of the obtained supernatant at 100,000 × *g* for 90 min (70-Ti rotor; Beckman, Milan, Italy) at 4°C resulted in the isolation of the ER (pellet) and cytosolic (supernatant) fractions. The crude mitochondrial fraction was resuspended in isolation buffer (250 mM mannitol, 5 mM HEPES, pH 7.4, and 0.5 mM EGTA) and then subjected to Percoll gradient centrifugation (Percoll medium: 225 mM mannitol, 25 mM HEPES, pH 7.4, 1 mM EGTA, and 30% [vol/vol] Percoll) in a 10-ml polycarbonate ultracentrifuge tube. After centrifugation at 95,000 × *g* for 30 min (SW40 rotor), a dense band containing purified mitochondria was recovered approximately three-fourths of the way down the tube. This was then washed by centrifugation at 6300 × *g* for 10 min to remove the Percoll and finally resuspended in isolation medium. The mitochondrial-associated membranes (MAMs), which contain the structural contacts between the mitochondria and the ER, were removed from the Percoll gradient as a diffuse white band located above the mitochondria, diluted in isolation buffer, and centrifuged at 6300 × *g* for 10 min. The supernatant was further centrifuged at 100,000 × *g* for 90 min (70-Ti rotor) to pellet the MAM fraction. When preservation of protein phosphorylation states was required, 2 mM Na_3VO_4 and 2 mM NaF were added to each fraction immediately after recovery.

Analysis of protein localization using a digitonin-based fractionation technique

Twenty-four hours posttransfection, confluent HeLa cells were trypsinized and harvested in cold PBS, pH 7.4, centrifuged at 750 × *g* for 5 min, washed in PBS, and permeabilized with digitonin for 20 min on ice after resuspension of the cell pellet in 200 μl of buffer I (150 mM NaCl, 50 mM HEPES, pH 7.4, 100 μg/ml digitonin) supplemented with protease and phosphatase inhibitors. After incubation on ice, plasma membrane permeabilization of cells was confirmed by staining with a 0.2% trypan blue solution. Cells were then centrifuged at 2000 × *g* for 5 min. The supernatants (cytosolic fractions) were saved, and the pellets were washed, solubilized in the same volume of buffer II (150 mM NaCl, 50 mM HEPES, pH 7.4, 1% NP-40) supplemented with complete protease inhibitor cocktail, vortexed, and incubated for 30 min on ice. After centrifugation at 7000 × *g* for 5 min to pellet nuclei and debris, the supernatants were kept as the heavy membrane fractions enriched for mitochondria. All steps were performed at 4°C. The soluble and heavy membrane fractions were separated by SDS–PAGE (4–12%) and transferred to a nitrocellulose membrane. After blocking nonspecific sites for 1 h at room temperature with 2.5% nonfat milk in PBS supplemented with 0.1% Tween-20, the nitrocellulose membranes were incubated overnight at 4°C with rabbit anti–Drp-1 (1:1000; Cell Signaling), rabbit anti-Mcl-1 (1:500; Santa Cruz Biotechnology), or β-tubulin (1:5000; Sigma-Aldrich) as a loading control. The immunoreactive proteins were then visualized using HRP-conjugated goat anti-mouse or anti-rabbit antibodies (1:5000) and enhanced chemiluminescence.

Immunoprecipitation

Cells were lysed in 3-[(3-cholamidopropyl)dimethylammonio]-1-propanesulfonate–based lysis buffer. Whole-cell lysates were obtained, precleared with protein A–Sepharose, and then incubated overnight with a 1:100 dilution of the specific antibody anti-Mcl-1. The immunocomplexes were captured with protein A. Beads were pelleted, washed three times, and boiled in SDS sample buffer. For the reverse immunoprecipitation, Drp1 was overexpressed in HeLa cells, and the antibody was cross-linked to protein A–agarose by

25 mM dimethyl pimelimidate. The presence of immune complexes was determined by Western blot analysis.

Statistical analysis and gel quantification

Statistical analysis was performed using Student's *t* test; $p < 0.05$ was considered significant. All data are reported as means ± SEs.

Quantification of Western blots was performed with ImageJ (National Institutes of Health, Bethesda, MD) to compare the density of bands on a gel.

ACKNOWLEDGMENTS

We thank Elena Marchesi and Lara Mari for excellent technical assistance with ASO synthesis and Gaia Pedriali for her help in performing experiments. P.P. is grateful to Camilla degli Scrovegni for continuous support. This work was funded by the Italian Association for Cancer Research (IG-14442 and MFAG-13521) and local funds from the University of Ferrara to P.P. and C.G. and Telethon (GGP11139B), the Italian Ministry of Health, and the Italian Ministry of Education, University and Research (COFIN 20129JLHSY_002, FIRB RBAP11FXBC_002, and Futuro in Ricerca RBFR10EGVP_001) to P.P.

REFERENCES

Akl H, Vervloessem T, Kiviluoto S, Bittremieux M, Parys JB, De Smedt H, Bultynck G (2014). A dual role for the anti-apoptotic Bcl-2 protein in cancer: mitochondria versus endoplasmic reticulum. Biochim Biophys Acta 1843, 2240–2252.

Bae J, Leo CP, Hsu SY, Hsueh AJ (2000). MCL-1S, a splicing variant of the antiapoptotic BCL-2 family member MCL-1, encodes a proapoptotic protein possessing only the BH3 domain. J Biol Chem 275, 25255–25261.

Bauman JA, Li SD, Yang A, Huang L, Kole R (2010). Anti-tumor activity of splice-switching oligonucleotides. Nucleic Acids Res 38, 8348–8356.

Bereiter-Hahn J, Voth M (1994). Dynamics of mitochondria in living cells: shape changes, dislocations, fusion, and fission of mitochondria. Microsc Res Tech 27, 198–219.

Bingle CD, Craig RW, Swales BM, Singleton V, Zhou P, Whyte MK (2000). Exon skipping in Mcl-1 results in a bcl-2 homology domain 3 only gene product that promotes cell death. J Biol Chem 275, 22136–22146.

Boise LH, Gottschalk AR, Quintans J, Thompson CB (1995). Bcl-2 and Bcl-2-related proteins in apoptosis regulation. Curr Top Microbiol Immunol 200, 107–121.

Bononi A, Bonora M, Marchi S, Missiroli S, Poletti F, Giorgi C, Pandolfi PP, Pinton P (2013). Identification of PTEN at the ER and MAMs and its regulation of Ca(2+) signaling and apoptosis in a protein phosphatase-dependent manner. Cell Death Differ 20, 1631–1643.

Bonora M, Bononi A, De Marchi E, Giorgi C, Lebiedzinska M, Marchi S, Patergnani S, Rimessi A, Suski JM, Wojtala A, *et al.* (2013a). Role of the c subunit of the FO ATP synthase in mitochondrial permeability transition. Cell Cycle 12, 674–683.

Bonora M, Giorgi C, Bononi A, Marchi S, Patergnani S, Rimessi A, Rizzuto R, Pinton P (2013b). Subcellular calcium measurements in mammalian cells using jellyfish photoprotein aequorin-based probes. Nat Protoc 8, 2105–2118.

Chao JR, Wang JM, Lee SF, Peng HW, Lin YH, Chou CH, Li JC, Huang HM, Chou CK, Kuo ML, *et al.* (1998). mcl-1 is an immediate-early gene activated by the granulocyte-macrophage colony-stimulating factor (GM-CSF) signaling pathway and is one component of the GM-CSF viability response. Mol Cell Biol 18, 4883–4898.

Chen H, Chomyn A, Chan DC (2005). Disruption of fusion results in mitochondrial heterogeneity and dysfunction. J Biol Chem 280, 26185–26192.

Chen TW, Wardill TJ, Sun Y, Pulver SR, Renninger SL, Baohan A, Schreiter ER, Kerr RA, Orger MB, Jayaraman V, *et al.* (2013). Ultrasensitive fluorescent proteins for imaging neuronal activity. Nature 499, 295–300.

Clohessy JG, Zhuang J, de Boer J, Gil-Gomez G, Brady HJ (2006). Mcl-1 interacts with truncated Bid and inhibits its induction of cytochrome c release and its role in receptor-mediated apoptosis. J Biol Chem 281, 5750–5759.

Derenne S, Monia B, Dean NM, Taylor JK, Rapp MJ, Harousseau JL, Bataille R, Amiot M (2002). Antisense strategy shows that Mcl-1 rather than Bcl-2 or Bcl-x(L) is an essential survival protein of human myeloma cells. Blood 100, 194–199.

Eckenrode EF, Yang J, Velmurugan GV, Foskett JK, White C (2010). Apoptosis protection by Mcl-1 and Bcl-2 modulation of inositol 1,4,5-trisphosphate receptor-dependent Ca2+ signaling. J Biol Chem 285, 13678–13684.

Fesik SW (2005). Promoting apoptosis as a strategy for cancer drug discovery. Nat Rev Cancer 5, 876–885.

Frank S, Gaume B, Bergmann-Leitner ES, Leitner WW, Robert EG, Catez F, Smith CL, Youle RJ (2001). The role of dynamin-related protein 1, a mediator of mitochondrial fission, in apoptosis. Dev Cell 1, 515–525.

Frezza C, Cipolat S, Martins de Brito O, Micaroni M, Beznoussenko GV, Rudka T, Bartoli D, Polishuck RS, Danial NN, De Strooper B, Scorrano L (2006). OPA1 controls apoptotic cristae remodeling independently from mitochondrial fusion. Cell 126, 177–189.

Galluzzi L, Bravo-San Pedro JM, Vitale I, Aaronson SA, Abrams JM, Adam D, Alnemri ES, Altucci L, Andrews D, Annicchiarico-Petruzzelli M, *et al.* (2015). Essential versus accessory aspects of cell death: recommendations of the NCCD 2015. Cell Death Differ 22, 58–73.

Giorgi C, Baldassari F, Bononi A, Bonora M, De Marchi E, Marchi S, Missiroli S, Patergnani S, Rimessi A, Suski JM, *et al.* (2012). Mitochondrial Ca(2+) and apoptosis. Cell Calcium 52, 36–43.

Giorgi C, Bonora M, Sorrentino G, Missiroli S, Poletti F, Suski JM, Galindo Ramirez F, Rizzuto R, Di Virgilio F, Zito E, *et al.* (2015). p53 at the endoplasmic reticulum regulates apoptosis in a Ca2+-dependent manner. Proc Natl Acad Sci USA 112, 1779–1784.

Gleave ME, Monia BP (2005). Antisense therapy for cancer. Nat Rev Cancer 5, 468–479.

Gunter TE, Pfeiffer DR (1990). Mechanisms by which mitochondria transport calcium. Am J Physiol 258, C755–786.

Hackenbrock CR (1966). Ultrastructural bases for metabolically linked mechanical activity in mitochondria. I. Reversible ultrastructural changes with change in metabolic steady state in isolated liver mitochondria. J Cell Biol 30, 269–297.

Hadaschik BA, Jackson J, Fazli L, Zoubeidi A, Burt HM, Gleave ME, So AI (2008). Intravesically administered antisense oligonucleotides targeting heat-shock protein-27 inhibit the growth of non-muscle-invasive bladder cancer. BJU Int 102, 610–616.

Hajnoczky G, Csordas G, Das S, Garcia-Perez C, Saotome M, Sinha Roy S, Yi M (2006). Mitochondrial calcium signalling and cell death: approaches for assessing the role of mitochondrial Ca2+ uptake in apoptosis. Cell Calcium 40, 553–560.

Hanada M, Delia D, Aiello A, Stadtmauer E, Reed JC (1993). bcl-2 gene hypomethylation and high-level expression in B-cell chronic lymphocytic leukemia. Blood 82, 1820–1828.

Hardwick JM, Youle RJ (2009). SnapShot: BCL-2 proteins. Cell 138, 404.

Hershko A, Ciechanover A (1998). The ubiquitin system. Annu Rev Biochem 67, 425–479.

James DI, Parone PA, Mattenberger Y, Martinou JC (2003). hFis1, a novel component of the mammalian mitochondrial fission machinery. J Biol Chem 278, 36373–36379.

Kelekar A, Thompson CB (1998). Bcl-2-family proteins: the role of the BH3 domain in apoptosis. Trends Cell Biol 8, 324–330.

Khoury JD, Medeiros LJ, Rassidakis GZ, McDonnell TJ, Abruzzo LV, Lai R (2003). Expression of Mcl-1 in mantle cell lymphoma is associated with high-grade morphology, a high proliferative state, and p53 overexpression. J Pathol 199, 90–97.

Kim DW, Kim JH, Park M, Yeom JH, Go H, Kim S, Han MS, Lee K, Bae J (2011). Modulation of biological processes in the nucleus by delivery of DNA oligonucleotides conjugated with gold nanoparticles. Biomaterials 32, 2593–2604.

Kim JH, Sim SH, Ha HJ, Ko JJ, Lee K, Bae J (2009). MCL-1ES, a novel variant of MCL-1, associates with MCL-1L and induces mitochondrial cell death. FEBS Lett 583, 2758–2764.

Koo T, Wood MJ (2013). Clinical trials using antisense oligonucleotides in duchenne muscular dystrophy. Hum Gene Ther 24, 479–488.

Kozopas KM, Yang T, Buchan HL, Zhou P, Craig RW (1993). MCL1, a gene expressed in programmed myeloid cell differentiation, has sequence similarity to BCL2. Proc Natl Acad Sci USA 90, 3516–3520.

Kuwana T, Bouchier-Hayes L, Chipuk JE, Bonzon C, Sullivan BA, Green DR, Newmeyer DD (2005). BH3 domains of BH3-only proteins differentially regulate Bax-mediated mitochondrial membrane permeabilization both directly and indirectly. Mol Cell 17, 525–535.

Kuwana T, Newmeyer DD (2003). Bcl-2-family proteins and the role of mitochondria in apoptosis. Curr Opin Cell Biol 15, 691–699.

Marchi S, Lupini L, Patergnani S, Rimessi A, Missiroli S, Bonora M, Bononi A, Corra F, Giorgi C, De Marchi E, *et al.* (2013). Downregulation of the mitochondrial calcium uniporter by cancer-related miR-25. Curr Biol 23, 58–63.
Marchi S, Marinello M, Bononi A, Bonora M, Giorgi C, Rimessi A, Pinton P (2012). Selective modulation of subtype III IP(3)R by Akt regulates ER Ca(2)(+) release and apoptosis. Cell Death Dis 3, e304.
Marchi S, Patergnani S, Pinton P (2014). The endoplasmic reticulum-mitochondria connection: one touch, multiple functions. Biochim Biophys Acta 1837, 461–469.
Marchi S, Pinton P (2014). The mitochondrial calcium uniporter complex: molecular components, structure and physiopathological implications. J Physiol 592, 829–839.
Maurer U, Charvet C, Wagman AS, Dejardin E, Green DR (2006). Glycogen synthase kinase-3 regulates mitochondrial outer membrane permeabilization and apoptosis by destabilization of MCL-1. Mol Cell 21, 749–760.
Minagawa N, Kruglov EA, Dranoff JA, Robert ME, Gores GJ, Nathanson MH (2005). The anti-apoptotic protein Mcl-1 inhibits mitochondrial Ca2+ signals. J Biol Chem 280, 33637–33644.
Mitra K, Wunder C, Roysam B, Lin G, Lippincott-Schwartz J (2009). A hyperfused mitochondrial state achieved at G1-S regulates cyclin E buildup and entry into S phase. Proc Natl Acad Sci USA 106, 11960–11965.
Opferman JT, Letai A, Beard C, Sorcinelli MD, Ong CC, Korsmeyer SJ (2003). Development and maintenance of B and T lymphocytes requires antiapoptotic MCL-1. Nature 426, 671–676.
Patergnani S, Giorgi C, Maniero S, Missiroli S, Maniscalco P, Bononi I, Martini F, Cavallesco G, Tognon M, Pinton P (2015). The endoplasmic reticulum mitochondrial calcium cross talk is downregulated in malignant pleural mesothelioma cells and plays a critical role in apoptosis inhibition. Oncotarget 6, 23427–23444.
Perciavalle RM, Opferman JT (2013). Delving deeper: MCL-1's contributions to normal and cancer biology. Trends Cell Biol 23, 22–29.
Perciavalle RM, Stewart DP, Koss B, Lynch J, Milasta S, Bathina M, Temirov J, Cleland MM, Pelletier S, Schuetz JD, *et al.* (2012). Anti-apoptotic MCL-1 localizes to the mitochondrial matrix and couples mitochondrial fusion to respiration. Nat Cell Biol 14, 575–583.
Pinton P, Giorgi C, Pandolfi PP (2011). The role of PML in the control of apoptotic cell fate: a new key player at ER-mitochondria sites. Cell Death Differ 18, 1450–1456.
Placzek WJ, Wei J, Kitada S, Zhai D, Reed JC, Pellecchia M (2010). A survey of the anti-apoptotic Bcl-2 subfamily expression in cancer types provides a platform to predict the efficacy of Bcl-2 antagonists in cancer therapy. Cell Death Dis 1, e40.
Renault TT, Floros KV, Elkholi R, Corrigan KA, Kushnareva Y, Wieder SY, Lindtner C, Serasinghe MN, Asciolla JJ, Buettner C, *et al.* (2014). Mitochondrial shape governs BAX-induced membrane permeabilization and apoptosis. Mol Cell 57, 69–82.
Rimessi A, Patergnani S, Bonora M, Wieckowski MR, Pinton P (2015). Mitochondrial Ca(2+) remodeling is a prime factor in oncogenic behavior. Front Oncol 5, 143.
Scarpa A, Azzone GF (1970). The mechanism of ion translocation in mitochondria. 4. Coupling of K+ efflux with Ca2+ uptake. Eur J Biochem 12, 328–335.
Scheckhuber C (2005). Mitochondrial dynamics in cell life and death. Sci Aging Knowledge Environ 2005, pe36.
Scorrano L (2013). Keeping mitochondria in shape: a matter of life and death. Eur J Clin Invest 43, 886–893.
Shieh JJ, Liu KT, Huang SW, Chen YJ, Hsieh TY (2009). Modification of alternative splicing of Mcl-1 pre-mRNA using antisense morpholino oligonucleotides induces apoptosis in basal cell carcinoma cells. J Invest Dermatol 129, 2497–2506.
Shin HW, Shinotsuka C, Torii S, Murakami K, Nakayama K (1997). Identification and subcellular localization of a novel mammalian dynamin-related protein homologous to yeast Vps1p and Dnm1p. J Biochem 122, 525–530.
Sieghart W, Losert D, Strommer S, Cejka D, Schmid K, Rasoul-Rockenschaub S, Bodingbauer M, Crevenna R, Monia BP, Peck-Radosavljevic M, Wacheck V (2006). Mcl-1 overexpression in hepatocellular carcinoma: a potential target for antisense therapy. J Hepatol 44, 151–157.
Skoda C, Erovic BM, Wachek V, Vormittag L, Wrba F, Martinek H, Heiduschka G, Kloimstein P, Selzer E, Thurnher D (2008). Down-regulation of Mcl-1 with antisense technology alters the effect of various cytotoxic agents used in treatment of squamous cell carcinoma of the head and neck. Oncol Rep 19, 1499–1503.
Skvara H, Thallinger C, Wacheck V, Monia BP, Pehamberger H, Jansen B, Selzer E (2005). Mcl-1 blocks radiation-induced apoptosis and inhibits clonogenic cell death. Anticancer Res 25, 2697–2703.
Smirnova E, Griparic L, Shurland DL, van der Bliek AM (2001). Dynamin-related protein Drp1 is required for mitochondrial division in mammalian cells. Mol Biol Cell 12, 2245–2256.
Spitali P, Aartsma-Rus A (2012). Splice modulating therapies for human disease. Cell 148, 1085–1088.
Suski JM, Lebiedzinska M, Bonora M, Pinton P, Duszynski J, Wieckowski MR (2012). Relation between mitochondrial membrane potential and ROS formation. Methods Mol Biol 810, 183–205.
Szabadkai G, Simoni AM, Chami M, Wieckowski MR, Youle RJ, Rizzuto R (2004). Drp-1-dependent division of the mitochondrial network blocks intraorganellar Ca2+ waves and protects against Ca2+-mediated apoptosis. Mol Cell 16, 59–68.
Thomas LW, Lam C, Edwards SW (2010). Mcl-1; the molecular regulation of protein function. FEBS Lett 584, 2981–2989.
Tondera D, Santel A, Schwarzer R, Dames S, Giese K, Klippel A, Kaufmann J (2004). Knockdown of MTP18, a novel phosphatidylinositol 3-kinase-dependent protein, affects mitochondrial morphology and induces apoptosis. J Biol Chem 279, 31544–31555.
van der Bliek AM (1999). Functional diversity in the dynamin family. Trends Cell Biol 9, 96–102.
Varadarajan S, Butterworth M, Wei J, Pellecchia M, Dinsdale D, Cohen GM (2013). Sabutoclax (BI97C1) and BI112D1, putative inhibitors of MCL-1, induce mitochondrial fragmentation either upstream of or independent of apoptosis. Neoplasia 15, 568–578.
Vinogradov A, Scarpa A (1973). The initial velocities of calcium uptake by rat liver mitochondria. J Biol Chem 248, 5527–5531.
Wacheck V, Cejka D, Sieghart W, Losert D, Strommer S, Crevenna R, Monia BP, Selzer E (2006). Mcl-1 is a relevant molecular target for antisense oligonucleotide strategies in gastric cancer cells. Cancer Biol Ther 5, 1348–1354.
Westrate LM, Sayfie AD, Burgenske DM, MacKeigan JP (2014). Persistent mitochondrial hyperfusion promotes G2/M accumulation and caspase-dependent cell death. PLoS One 9, e91911.
Wieckowski MR, Giorgi C, Lebiedzinska M, Duszynski J, Pinton P (2009). Isolation of mitochondria-associated membranes and mitochondria from animal tissues and cells. Nat Protoc 4, 1582–1590.
Yang T, Kozopas KM, Craig RW (1995). The intracellular distribution and pattern of expression of Mcl-1 overlap with, but are not identical to, those of Bcl-2. J Cell Biol 128, 1173–1184.
Yin XM, Oltvai ZN, Korsmeyer SJ (1994). BH1 and BH2 domains of Bcl-2 are required for inhibition of apoptosis and heterodimerization with Bax. Nature 369, 321–323.
Yoon Y, Pitts KR, McNiven MA (2001). Mammalian dynamin-like protein DLP1 tubulates membranes. Mol Biol Cell 12, 2894–2905.